



Composite Multiaxial Mechanics: Laminate Design Optimization of Taper-Less Wind Turbine Blades with Ramie Fiber-Reinforced Polylactic Acid

Ardy Lololau¹, Tresna Priyana Soemardi^{1*}, Harry Purnama², Olivier Polit³

¹*Department of Mechanical Engineering, Faculty of Engineering, Universitas Indonesia, Kampus UI Depok, Depok 16424, Indonesia*

²*Center of Technology for Machinery Industry, TIRBR, BPPT Serpong, Tangerang 15314, Indonesia*

³*Laboratoire Energétique Mécanique Electromagnétisme, Université Paris Ouest, Ville d'Avray, 92410, France*

Abstract. As the research on composite materials based on natural resources proliferates further, ramie fiber and polylactic acid (PLA), which are fully biodegradable composite materials, are expected to be used for mechanical application due to their excellent strength and degradability. Various natural fibers have been applied to a wind turbine blade composite structure, as reinforcement material. However, none of them are fully biodegradable, as the matrix still uses synthetic resins. Hence, this study aims to theoretically optimize the fully biodegradable ramie/PLA laminate design using its lamina orientation on a taper-less blade shell of a wind turbine, as the operating structure experienced multiaxial loading through bending and torsional moment derived by the wind. The selection of taper-less blades was made due to their congruence with the wind speed categorization in southeastern Indonesian territory. The optimization was carried out using the nonlinear Generalized Reduced Gradient (GRG) method on Microsoft Excel. The optimized laminate result is in a stacking sequence of $[-4^\circ, 24^\circ, 47^\circ, 65^\circ, 74^\circ, 79^\circ]_s$ that delivers the factor of safety, which is the ratio between the allowable stress and the actual stress, of 7.296 and 18.057 on the longitudinal axis and the laminate shear-plane, respectively. This renders the composite laminate highly safe, both theoretically and numerically.

Keywords: Composite laminate optimization; Multiaxial loading; Polylactic acid; Ramie fiber; Taper-less blade

1. Introduction

Fiber-reinforced composites have been used as an alternative material in many mechanical applications because their specific strength and stiffness are superior to other engineering materials in general. The development of fiber-reinforced composites in Indonesia has reached an advanced stage, especially in relation to natural fibers (Shieddieque et al., 2021). The use of natural fibers in reinforcing polymer composite materials offers several advantages, since they have low density and are biodegradable, inexpensive, and renewable (Pickering et al., 2016; Rohan et al., 2018).

One of the natural fibers that can be utilized as a reinforcement of polymer composites is ramie fiber. Ramie fiber reinforcement in composites has been utilized in various applications, such as LPG tanks and bulletproof panels (Saidah, 2004; Suryaneta, 2007). Meanwhile, the use of polylactic acid (PLA) as a composite matrix is being intensively

*Corresponding author's email: tsoemardi@eng.ui.ac.id, Tel.: +62-81-6824490; Fax.: +62-21-727-0032
doi: [10.14716/ijtech.v12i6.5199](https://doi.org/10.14716/ijtech.v12i6.5199)

pursued in an effort to implement the Green Composite campaign.

PLA is also considered to be able to compete with synthetic (conventional) matrices because of its relatively good strength, having a tensile strength of 50.75 MPa and a tensile modulus of 3.5 GPa (Sawpan et al., 2007). With this potential, PLA and ramie fiber should be used to subvert the domination of synthetic material in the composite field for mechanical applications. However, PLA has experienced a critical decline in its mechanical properties (strength, modulus, toughness) during weather degradation. For example, PLA underwent a 92% decrease in tensile strength (Varsavas and Kaynak, 2018). Additionally, the water absorption will increase, and the microorganisms will be attracted by the addition of natural fibers in PLA composites, which will assist in the hydrolysis of polymers and enhance the degradation rate of the composites (Surip et al., 2018). This indicates that PLA has good biodegradability. PLA is also commercially attractive, especially in developing countries and high-plastic-consumption countries such as Indonesia. PLA has a low melting point of 150 °C, which makes the energy requirements and greenhouse gas emissions low during preparation. Hence, the low melting point indicates good manufacturability, which will enable many preparation methods, such as extrusion, injection molding, hot pressing, film stacking, and pultrusion (Rajeshkumar et al., 2021).

PLA and ramie fiber have also been considered to be the most common natural or bio-composite material pair. The research on these natural material pairs has been conducted via various experimental studies, which have also indicated that most bio-composite, especially ramie/PLA, requires pre-treatment to enhance their mechanical behavior, whether through chemical compound pre-treatment (Yu et al., 2015; Fatra et al., 2016) or pre-loading treatment (Zhou et al., 2013). Ramie/PLA composites also exhibit good water absorption but lower moisture absorption when pre-impregnated in hybrid-woven yarn with different weaving patterns (Baghaei et al., 2015).

Despite their excellent characteristics, composite is susceptible to fatigue and fracture phenomena when subjected to specific cyclic loads (static or dynamic) and environmental factors (temperature and corrosive media). Therefore, an understanding and prediction of the further propagation of such defects are of paramount importance. Furthermore, the failure mechanism of fiber-reinforced composites is more complicated when subjected to multiaxial (tension torsion) loading than when subjected to uniaxial loading, signifying that there is a solid interaction between axial stress and shear stress when the failure occurs (Lee et al., 1999). A multiaxial fatigue strain energy density has been contributed by the stresses and strains on the critical or fracture plane under various mean stress levels and loading combinations (Glinka et al., 1995). Consequently, experimental research under various complex loading conditions is mandatory to generate testing conditions which approximate reality to apply the damage criteria appropriately (Bathias et al., 1992; Quaresimin et al., 2015). Hence, the prediction of the multiaxial behavior of ramie/PLA composite has been estimated semi-empirically before on thin-walled tube laminate with a load of uniaxial tension-compression, torsion, and internal pressure. The results semi-empirically demonstrate that with a 26% reinforcing volume fraction, the composite laminate can retain a maximum longitudinal stress of 120.5 MPa and a maximum in-plane shear stress of 13.03 MPa in the failure criteria envelope (Lololau, 2021).

On the other hand, Indonesia is a country with high wind energy potential, especially in the southeastern territory, which devotes an average windspeed of 7.5-8 m/s and a maximum of 12 m/s to wind farms (Satwika et al., 2019; Hesty et al., 2021). The use of wind energy in Indonesia is arguably still lacking the technology to achieve what is desired, but in reality, only a handful of people have used wind energy. One method to capture wind energy is to use wind turbines. Wind turbines generally used in Indonesia are horizontal axis wind

turbines with three propellers (Yohana et al., 2020). In wind turbines, the first component interacting directly with wind energy is the blades. Designing a wind turbine blade with a good power coefficient is strongly influenced by the blade's geometry. One significant geometric parameter is the blade's width. A blade with a taper-less type is a blade with a uniform blade width from the base to the blade's tip. This type of blade is suitable for wind turbines with regional manifestations with medium wind speeds of 5-8 m/s (National Weather Service Portland, nd), which applies to many regions in Indonesia.

What then becomes a challenge is applying composite materials to these taper-less blades so that the blades obtained are lighter and have high strength according to the desired design. Composite materials have been used in wind turbine blade application for decades but mainly consist of conventional synthetic constituents, such as glass fiber, carbon fiber, and epoxy (Mishnaevsky et al., 2017). Therefore, it is necessary to alter it with biodegradable ones to address the disposal problem that has been a source of disruption for years. Several natural fibers, such as flax, jute, coir, and sisal, have been applied experimentally on a wind turbine blade structure in combination with glass fiber and epoxy resin matrix (Kalagi et al., 2018; Li et al., 2020). Hence, to the author's knowledge, no fully natural or bio materials used as composite are applied to the wind turbine blade structure.

On the other hand, when converting wind energy into electrical energy, the blades on a horizontal axis wind turbine generally experience two main loads, namely bending and torsional moment (Piggott, 1997; Ghasemi and Mohandes, 2016). This multiaxial load must be understood and considered before applying these bio-composite materials to the taper-less blade structure. Therefore, it is at least necessary to optimize both theoretically and numerically as a first step to the composite laminate design so that the bio-composite has an effective performance when receiving multiaxial loads that occur in the taper-less blade structure.

Against this background, the research has been undertaken to theoretically or empirically optimize the ramie-reinforced PLA bio-composite laminate design based on their factor of safety applied on multiaxial-loaded taper-less wind turbine blades. It suggests that this optimization would produce a safer design for novel ramie-reinforced PLA taper-less wind turbine blade composite laminate to be manufactured in future projects. In the long term, this research will establish the potential of ramie fiber-reinforcing material in PLA composites as a material used for mechanical products. This study was also a part of the author's Ramie Fiber-Reinforced PLA (RFRPLA) prepregs development research to determine the mechanical multiaxial characteristics of applying it to automotive, aeronautic, and power plant structure components with 1:1 component realization or slightly smaller.

2. Methods

2.1. Blade Design

The designed blade structure is a blade of a taper-less type that uses a National Advisory Committee for Aeronautics (NACA) 4412 airfoil (Figure 1; Thickness 0.12 at 0.291; Camber 0.04 at 0.395; 34 points). If the electrical power capacity to be achieved is 500 Watts, and the efficiency of each component starting from the blades, transmission, generator, and controller is 0.3-0.4, 0.9, 0.9, and 0.9, respectively, while the maximum wind speed that the blades can capture is 12 m/s, then the required length of the blade l is 0.8 m (Piggott, 1997; Yohana et al., 2020; Ravianto, 2021). The rotor used consists of three blades with a width b of 0.16 m, assuming the tip speed ratio (TSR) is 7.

The blades will then be partitioned into 11 posts, which will be used in aerodynamic flow simulation using QBlade software (v0.8 on XFLR5 v6.06; HFI TU Berlin; Müller-

Breslau-Straße 8, D-10623 Berlin; Germany).

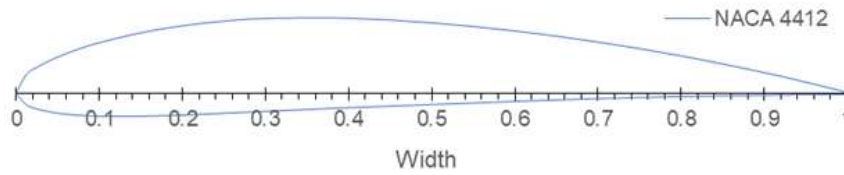


Figure 1 NACA 4412 Airfoil

The simulation parameter and setting can be seen in Table 1. NACA 4412 is used because it has a high lift coefficient to drag coefficient ratio, 133.64 (Ockfen and Matveev, 2009). The eleven partitioned posts have different lift coefficients. Subsequently, the angle of attack can be identified through the simulation results graph on the QBlade. Ultimately, the twist angle per blade partition post can be known and linearized. The rotor is then modelled on QBlade for multiparameter simulation, as shown in Figure 2.

Table 1 Q-Blade aerodynamical simulation parameters and settings

Parameter	Value	Unit	Parameter	Value	Unit
ρ	1.225	kg/m ³	Rotational speed range (Start)	50	1/m
η	1.78×10^{-5}	kg/(m.s)	Rotational speed range (End)	1000	1/m
Relax factor	0.3		Rotational speed range (Delta)	50	1/m
Max. iteration	1000		Pitch range (Start)	7.75	°
Element	20		Pitch range (End)	13	°
Epsilon	0.001		Pitch range (Delta)	0.25	°
Wind speed range (Start)	1	m/s			
Wind speed range (End)	12	m/s			
Wind speed range (Delta)	1	m/s			

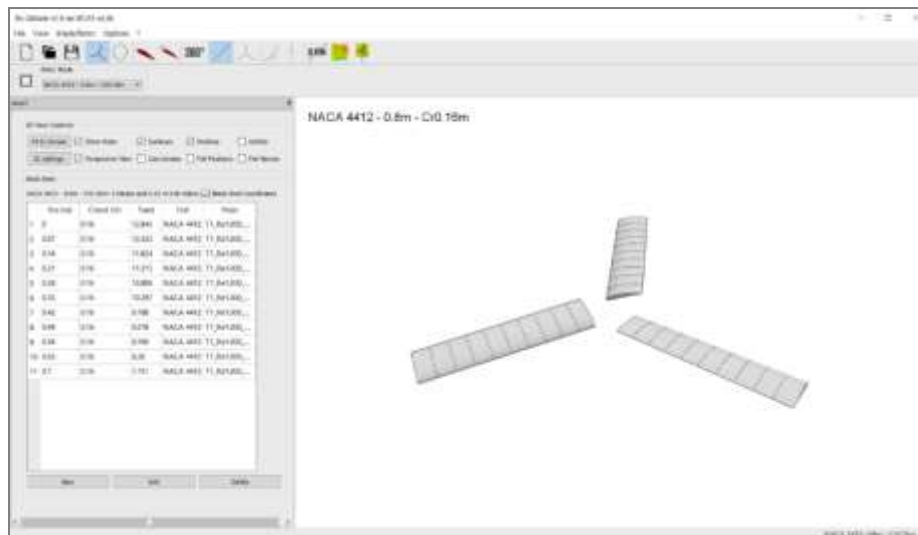


Figure 2 Rotor blade design on QBlade

After performing a multiparameter simulation, the highest torque T occurred to the pitch of 7.75° (tip of the blade), and the wind speed of 12 m/s that occurred on the blade is 25.5 Nm with a bending moment M , which also occurred at 17.15 Nm, as seen in Figure 3. It can be assumed that the torque and bending moment that occurred at the blade is directly proportional to the wind speed, as a lower wind speed will exhibit a lower torque and bending moment.

The stresses as a result of the bending moment and torsion that occurred on the blade are then calculated, namely the bending stress $\sigma_{bending\ actual}$ and shear stress τ_{actual} which can be described as follows:

$$\sigma_{bending\ actual} = \frac{M c}{I} \tag{1}$$

Where c is the maximum camber of the airfoil of 6.4 mm, and

$$I = 0.036 b f (f^2 + c^2) \tag{2}$$

Where f is the thickness of the airfoil, which is 19.23 mm. While:

$$\tau_{actual} = \frac{2T}{0.6 b^2 f} \tag{3}$$

Thus, the actual value of bending stress is 2.423 MPa, and the actual shear stress is 0.173 MPa.

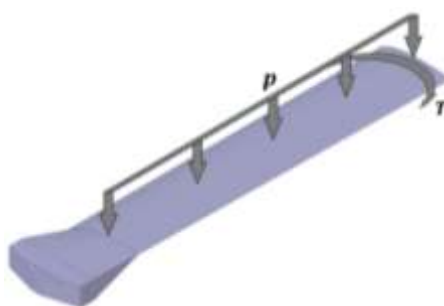


Figure 3 Loading on the taper-less blade

2.2. Mechanics of Composite Materials Modeling

The mechanics of composite material modeling were conducted based on a second edition book by Autar Kaw (2006) entitled “Mechanics of Composite Materials” (Kaw, 2006). The model was programmed on Microsoft Excel. The modeling was applied from both constituents to the unidirectional lamina model, then to the laminate through ABD coupling matrices theory, and then multiaxially loaded on the taper-less blade shell structure.

The ramie and PLA properties data used in this modeling were derived from Lololau (2021). Table 2 and Table 3 show the mechanical properties of flax and PLA, respectively.

Table 2 Properties of ramie (Lololau, 2021)

Properties	Mean value	Unit
ρ_f	1.50	gr/cc
$(\sigma_1^T)_f$	391.54	MPa
E_f	15.42	GPa
ν_f	0.2	

Table 3 Properties of PLA (Lololau, 2021)

Properties	Mean value	Unit
ρ_m	1.27	gr/cc
$(\sigma_1^T)_m$	20.32	MPa
E_m	1.71	GPa
ν_m	0.31	
$(\sigma_1^C)_m$	90.14	MPa
$(\tau_{12})_m$	21.22	MPa

Based on these properties and using the 45% volume fraction of the reinforcement, the theoretical stiffness engineering constants of the ramie/PLA unidirectional lamina are known to be as follows:

$$\begin{aligned}
 E_1 &= 7.90 \text{ GPa} & G_{23} &= 1.22 \text{ GPa} \\
 E_2 = E_3 &= 2.91 \text{ GPa} & \nu_{12} = \nu_{13} &= 0.26 \text{ GPa} \\
 G_{12} = G_{13} &= 1.12 \text{ GPa} & \nu_{23} &= 0.39 \text{ GPa}
 \end{aligned}$$

Thus, the theoretical ultimate strength of the ramie/PLA lamina can also be determined as follows:

$$\begin{aligned} (\sigma_1^T)_{ult} &= 200.65 \text{ MPa} & (\sigma_2^C)_{ult} &= 90.56 \text{ MPa} \\ (\sigma_1^C)_{ult} &= 82.61 \text{ MPa} & (\tau_{12})_{ult} &= 9.35 \text{ MPa} \\ (\sigma_2^T)_{ult} &= 7.90 \text{ MPa} \end{aligned}$$

Because the wind turbine blades are faced with dynamic loads corresponding to the fluctuation of the wind per usual, in which the structure will mostly fail due to fatigue, it can be assumed that the value of the allowable stress obtained through the lamina failure envelope will use its endurance limit value, which in most natural composite cases is about 25% of the ultimate strength (Mahboob and Bougherara, 2018; Feng et al., 2020) of the lamina for design safety, so that:

$$\begin{aligned} X &= \frac{(\sigma_1^T)_{ult}}{4} = 50.16 \text{ MPa} & Y^C &= \frac{(\sigma_2^C)_{ult}}{4} = 22.64 \text{ MPa} \\ X^C &= \frac{(\sigma_1^C)_{ult}}{4} = 20.65 \text{ MPa} & S &= \frac{(\tau_{12})_{ult}}{4} = 2.34 \text{ MPa} \\ Y &= \frac{(\sigma_2^T)_{ult}}{4} = 1.98 \text{ MPa} \end{aligned}$$

Furthermore, it is also known that the invariant forms used to calculate the stiffness matrix of the lamina are a function of the orientation of the lamina itself, where:

$$\begin{aligned} U_1 &= 4.91 \text{ GPa} & U_3 &= 0.63 \text{ GPa} \\ U_2 &= 2.56 \text{ GPa} & U_4 &= 1.41 \text{ GPa} \end{aligned}$$

The composite laminate designed on the blades of this taper-less wind turbine has an overall thickness of h 4.8 mm, consisting of 12 layers of lamina N . This results in a thickness per lamina t of 0.4 mm.

Given the assumptions and designs described in Section 2.1, it is known that the blade will experience the highest torque T at a wind speed of 12 m/s for a pitch of 7.75° (blade tip) of 25.5 Nm with a bending moment M , which also occurs at 17.15 Nm. Therefore, the torsion and bending moment occurring in these blades act as N_{xy} and M_x loadings on the designed global plane of the composite laminate, respectively, which produces the following matrix:

$$\begin{bmatrix} N_x \\ N_y \\ N_{xy} \\ M_x \\ M_y \\ M_{xy} \end{bmatrix} = \begin{bmatrix} 0 \\ 0 \\ N_{xy} \\ M_x \\ 0 \\ 0 \end{bmatrix}$$

where,

$$N_{xy} = \tau_{actual} h \quad (4)$$

and,

$$M_x = \frac{M}{l} \quad (5)$$

which will make:

$$\begin{bmatrix} N_x \\ N_y \\ N_{xy} \\ M_x \\ M_y \\ M_{xy} \end{bmatrix} = \begin{bmatrix} 0 \\ 0 \\ 8.29 \times 10^{-7} \\ 2.14 \times 10^{-8} \\ 0 \\ 0 \end{bmatrix} \begin{bmatrix} \text{GN/m} \\ \text{GN/m} \\ \text{GN/m} \\ \text{GNm/m} \\ \text{GNm/m} \\ \text{GNm/m} \end{bmatrix}^T$$

To provide factual information that states when a lamina in a laminate is declared to

fail, an absolute nominal is needed to describe it. Strength ratio (SR) is a comparison value between the maximum load that can be applied to a lamina and the actual load given. By applying the failure criterion theory of Tsai-Wu (Hoffman), the strength ratio value can be described as follows (Lololau, 2021):

$$SR = -\frac{(H_1\sigma_1 + H_2\sigma_2 + H_6\tau_{12})}{2(H_{11}\sigma_1^2 + H_{22}\sigma_2^2 + H_{66}\tau_{12}^2 + 2H_{12}\sigma_1\sigma_2)} + \frac{\sqrt{(H_1\sigma_1 + H_2\sigma_2 + H_6\tau_{12})^2 + 4(H_{11}\sigma_1^2 + H_{22}\sigma_2^2 + H_{66}\tau_{12}^2 + 2H_{12}\sigma_1\sigma_2)}}{2(H_{11}\sigma_1^2 + H_{22}\sigma_2^2 + H_{66}\tau_{12}^2 + 2H_{12}\sigma_1\sigma_2)} \quad (6)$$

Where the lamina on a laminate with the lowest SR value will fail because it has the highest F_I failure index value. The failure index itself is a scalar quantity that will indicate the lamina's failure that comprises a composite laminate. The failure index value can be described as follows (Narsai et al., 2018):

$$F_I = \frac{1}{SR^2} \quad (7)$$

2.3. Optimization

In this study, optimization was conducted on the orientation of each lamina θ (variable) to form a symmetrical and balanced laminate (constraint) and fulfill the condition, which has a maximum safety factor on the longitudinal axis of the composite laminate SF_x (objective), with the condition that the safety factor on the transverse axis of the composite laminate SF_y has a value of 1.5. This optimization is executed using the solver add-in in Microsoft Excel. This solver uses the nonlinear Generalized Reduced Gradient (GRG) method (Bharathiraja et al., 2017; Al-Fatlawi et al., 2021) to find the lamina orientations that produce the maximum factor of safety.

The initial value of the lamina orientation is based on the conventional stacking sequence of balance and symmetrical laminate of $[0^\circ, 90^\circ, 0^\circ, 90^\circ, 45^\circ, -45^\circ]_S$ which had the factor of safety SF_x of 4.658, SF_y of 1.5, and SF_{xy} of 20.514. This laminate also had effective stiffness engineering constants as follows:

$$\begin{aligned} \overline{E_x} = \overline{E_y} &= 4.84 \text{ GPa} \\ \overline{G_{xy}} &= 1.54 \text{ GPa} \\ \overline{\nu_{xy}} = \overline{\nu_{yx}} &= 0.23 \end{aligned}$$

The safety factor value itself (in this case study) is defined as the ratio between the maximum allowable stresses obtained in the lamina failure envelope to the stresses that occur in the global axis of the composite laminate. The stresses in the composite laminate's global axis occur due to torsion and bending moment in the blade structure. In contrast, the maximum allowable stresses obtained in the lamina failure envelope were derived based on the Hoffman failure criterion theory.

Hoffman's failure criterion itself has been found to be the most accurate and most conservative criterion (Narsai et al., 2018). This lamina failure envelope is also formed with the assumption that the allowable stress of the transverse axis of the composite laminate on the failure envelope is a constant value of 1.5 of the global transverse stress of the composite laminate. The value of the safety factor can be described as follows:

$$SF_x = \frac{(\sigma_1)_{max.allowable}}{\sigma_x} \quad (8)$$

$$SF_y = 1.5 \quad (9)$$

$$SF_{xy} = \frac{(\tau_{12})_{max.allowable}}{\tau_{xy}} \quad (10)$$

To ensure that the stacking sequence of the lamina based on the orientation is symmetrical and balanced, the difference in the magnitude of the orientation angle of the

n -th outermost lamina from the central plane of the laminate must be zero. To simplify the fabrication later, the value of the optimized lamina orientation angle must be an integer with a value of $-90 < \theta \leq 90$.

2.4. Finite Element Analysis (FEA) Simulation

The finite element analysis simulation had to be done to numerically validate the theoretically optimized laminate on their global and principal stress. The FEA result may also be plotted in the failure envelope to determine whether the stress that occurs in the structure is still included in the safety locus. The three-dimensional model of a wind turbine blade has been created on SolidWorks software (2012 version (version number 20); Dassault Systèmes; Massachusetts; United States). Meanwhile, the three-dimensional model itself will then be simulated with torsional loading and bending moments on Abaqus software (v6.10; ABAQUS Inc.; Rhode Island; United States). The selection of turbine blade static analysis ignores the laws of motion in the total time adjusted for the results of previous theoretical calculations.

The elements used in this simulation are S4R shell elements with a mesh size of 2 mm (obtained from convergency study in Figure 4 (as the normal stress value became constant)), resulting in a total of 68,735 elements and 68,902 nodes (Figure 5). The loading involves two variables: a bending moment of 17,150 Nmm and a torque of 25,500 Nmm, where the loading location is at the top end of the turbine blade (RP-1). At the same time, at the base part, it is held in a fixed condition (no displacement in any direction). Details regarding loading and constraint can be seen in Figure 6.

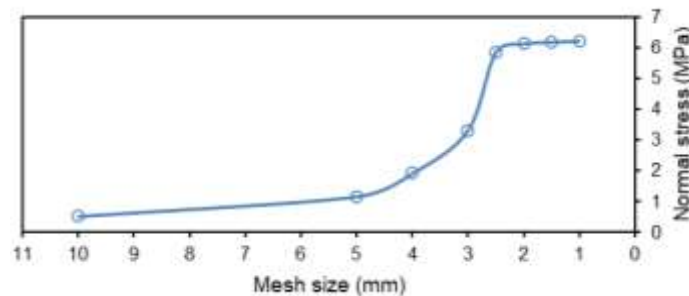


Figure 4 Meshing convergency study graph of the three-dimensional model of taper-less wind turbine blade

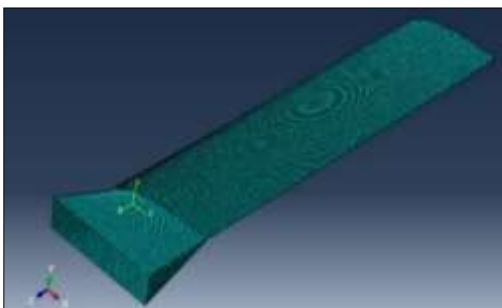


Figure 5 Meshing of the three-dimensional model of taper-less wind turbine blade

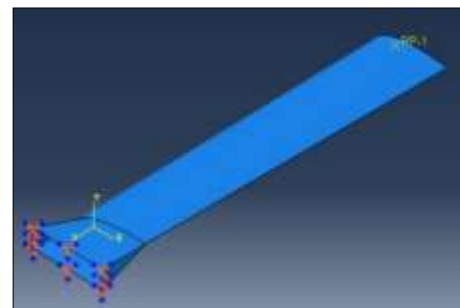


Figure 6 Loading and constraint of the three-dimensional model of taper-less wind turbine blade

3. Results and Discussion

3.1. Mechanics and Optimization

After the Microsoft Excel solver solved the optimization, the results indicate that the stacking sequence of the lamina that produces the maximum factor of safety on the

longitudinal axis of the laminate is $[-4^\circ, 24^\circ, 47^\circ, 65^\circ, 74^\circ, 79^\circ]_S$ with SF_x and SF_{xy} are 7.296 and 18.057, respectively, based on the torsional loading and bending moment on the blade structure.

Based on the optimization results, the laminate’s effective stiffness engineering constant is produced as follows:

$$\begin{aligned} \overline{E}_x &= 4.28 \text{ GPa} & \overline{\nu}_{xy} &= 0.22 \\ \overline{E}_y &= 4.61 \text{ GPa} & \overline{\nu}_{yx} &= 0.23 \\ \overline{G}_{xy} &= 1.49 \text{ GPa} & & \end{aligned}$$

As per the initial unoptimized value, this optimized laminate produced lower stiffness. This indicates that there always be a risk in optimizing a single objective of a value. Hence, indeed, it will require further optimization with multi-objectives in future projects. But if this effective engineering constant is compared to the result derived experimentally by (Kalagi et al., 2018), the Young modulus (assumed as \overline{E}_x) is superior to the three tested specimen types. Additionally, to point out that the precursor’s stacking layup is not the same and that it still uses conventional synthetic resin as a matrix, it is worth noting that it will bring the potential and advantage of ramie/PLA to establish as a prominent pair in natural or bio-composite material applications. After all, this study still requires experimental verification.

Additionally, as a result of torsional loading and bending moments that occur in the taper-less wind turbine blade structure, the strains, curvatures, and stresses that occur in the global composite laminate planar are as follows:

$$\begin{bmatrix} \varepsilon_x^0 \\ \varepsilon_y^0 \\ \gamma_{xy}^0 \\ \kappa_x \\ \kappa_y \\ \kappa_{xy} \end{bmatrix} = \begin{bmatrix} -7.05 \times 10^{-6} \\ -1.79 \times 10^{-5} \\ 1.16 \times 10^{-4} \\ 0.4 \\ -1.23 \times 10^{-1} \\ -9.35 \times 10^{-2} \end{bmatrix} \begin{bmatrix} m/m \\ m/m \\ m/m \\ 1/m \\ 1/m \\ 1/m \end{bmatrix}^T$$

$$\begin{bmatrix} \varepsilon_x \\ \varepsilon_y \\ \gamma_{xy} \end{bmatrix} = \begin{bmatrix} 1.91 \\ -0.61 \\ -0.33 \end{bmatrix} \times 10^{-3}$$

$$\begin{bmatrix} \sigma_x \\ \sigma_y \\ \tau_{xy} \end{bmatrix} = \begin{bmatrix} 7.922 \\ -1.048 \\ -0.177 \end{bmatrix} \text{ MPa}$$

Figure 7 illustrates a Hoffman’s lamina failure envelope with a constant allowable transverse stress of -1.57 MPa, which is 1.5 of the global transverse stress of the composite laminate.

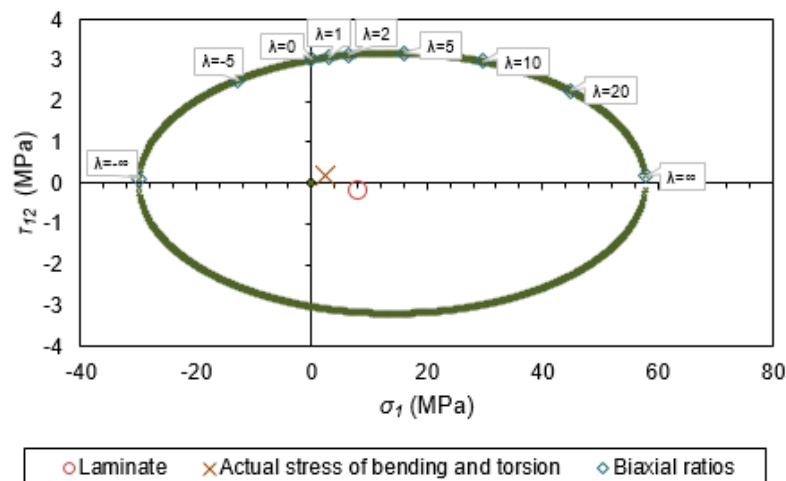


Figure 7 Hoffman’s lamina theoretical failure envelope for constant transverse stress of -1.57 MPa

Failure envelope is commonly used to show the maximum allowable stress that can occur in a certain material or structure before it experiences a failure. The locus generated

in the failure envelope indicates its boundary limit. The value of scattering outside of it is considered a failure. Therefore, from this failure envelope, it is evident that the maximum allowable longitudinal stress of the lamina $(\sigma_1)_{max.allowable}$ is 57.8 MPa occurs when the biaxial ratio λ is equal to ∞ (≈ 344.23), while the in-plane shear $(\tau_{12})_{max.allowable}$ is 3.187 MPa occurs when λ is equal to 5 (≈ 4.99). The biaxial ratio itself is the ratio between longitudinal stress and the shear stress (Lololau, 2021). There is also a scatter point in the failure envelope that indicates the laminate's global longitudinal and shear stress condition. It is still included in the locus of the failure envelope, which indicates that the composite laminate is safe when it receives torsional loading and bending moments on the blade structure, even on the actual biaxial bending and torsional stress, regardless of the optimized factor of safety value. The designation of Figure 7 directly indicates the safety of the blade design in the locus of its materials' allowable stresses.

Table 4 indicates the values of global and principal stresses that occur in each of the laminates that comprise the composite laminate. The values of these principal stresses are then compared with the finite element numerical simulation results on a three-dimensional model of this taper-less wind turbine blade.

Table 4 Global and principal stresses in each lamina

Ply no.-	θ (°)	σ_x	σ_y	τ_{xy}	σ_{max}	σ_{min}	τ_{max}
		MPa					
1	-4	15.023	-0.291	-1.053	15.095	-0.363	7.729
2	24	11.113	0.797	2.215	11.568	0.342	5.613
3	47	6.220	0.709	0.647	6.295	0.634	2.831
4	65	4.995	-1.564	-0.913	5.120	-1.689	3.404
5	74	5.049	-2.739	-1.040	5.185	-2.876	4.031
6	79	5.132	-3.201	-0.915	5.232	-3.300	4.266
7	79	5.132	-3.201	-0.915	5.232	-3.300	4.266
8	74	5.049	-2.739	-1.040	5.185	-2.876	4.031
9	65	4.995	-1.564	-0.913	5.120	-1.689	3.404
10	47	6.220	0.709	0.647	6.295	0.634	2.831
11	24	11.113	0.797	2.215	11.568	0.342	5.613
12	-4	15.023	-0.291	-1.053	15.095	-0.363	7.729
Total		95.066	-12.579	-2.118	58.913	-13.429	36.171
Average		7.922	-1.048	-0.177	7.364	-1.679	4.521

According to the failure criterion of a laminate theory, based on Hoffman's modification, the laminate will globally be damaged with a lamina sequence of 79°, -4°, 74°, 65°, 24°, and 47°, acknowledging the damage phenomena of ply-per-ply failure. The 79° laminas will be the first ply to fail, as the strength ratio shows the smallest number, and the failure index designates the greatest number, as seen in Table 5. Meanwhile, the 47° laminas will be the last ply to fail, as the strength ratio shows the largest number, and the failure index designates the most insignificant number.

Table 5 Strength ratio, failure index, and sequence of failure of taper-less blade ramie/PLA laminate

Ply angles (°)	No. of ply	σ_1	σ_2	τ_{12}	Strength ratio	Failure index	Sequence of failure
		MPa					
-4	2	15.095	-0.363	0.023	0.197	25.802	2
24	2	11.052	0.858	-2.351	1.167	0.734	5
47	2	3.918	3.011	-2.794	1.292	0.599	6
65	2	-1.092	4.523	-1.926	0.508	3.870	4
74	2	-2.699	5.008	-1.181	0.259	14.903	3
79	2	-3.240	5.172	-0.713	0.188	28.421	1

On the other hand, if this damaging phenomenon is considered in the fully discounted method (Kaw, 2006) proposed, the failure sequence is slightly different from the earlier one. What makes it different is the 24° lamina is found to be the last ply to fail, while the 47° lamina is the second to last. The approach of this method entirely relies upon the reduced ABD matrices, as the effective stiffness of the laminate has degraded through every phase of this damage phenomena, as the laminate lost its stiffness contributed by the failed ply. Figure 8 and Figure 9 illustrate the global stress and strain evolution during the damage phenomena as an indication of the stiffness degradation experienced by the taper-less blade laminate.

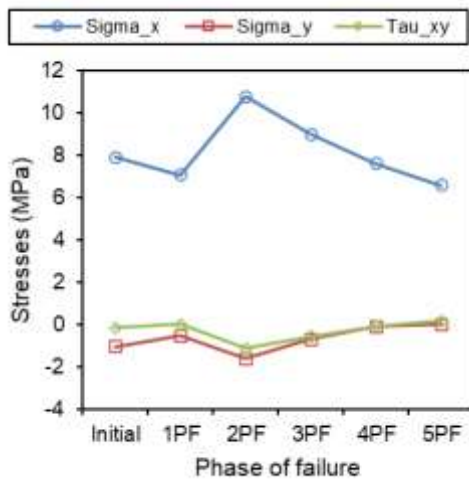


Figure 8 Global stress evolution during the damage phenomena

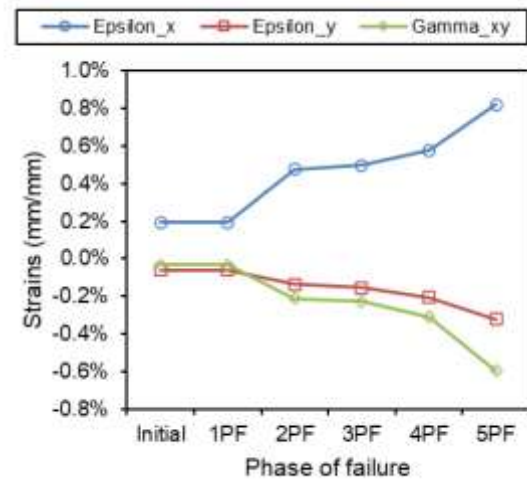


Figure 9 Global strains evolution during the damage phenomena

3.2. FEA

The simulation running process was performed on a laptop computer with an Intel i5 CPU specification with 16 GB RAM with an estimated time of about 16 hours. In addition to theoretical computations, composite laminates on a taper-less wind turbine blade structure are stacked in an optimized orientation, each with a thickness of 0.4 mm per lamina, as shown in Figure 10 below.

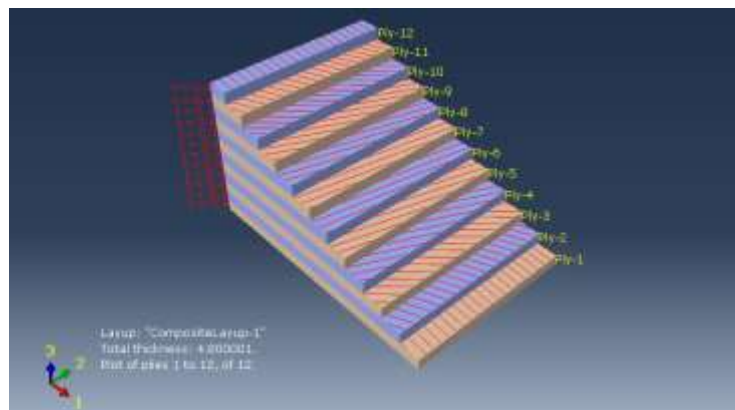


Figure 10 Laminate stacking sequence

Table 5 indicates the results of the numerical simulation of the finite element on Abaqus. There are still errors in the global and principal stress values from the simulation results. The difference with the theoretical computed stress values may be caused by the assumptions of equations in the simulation using more complex equations and discretization problems of equations of a model and its boundary conditions.

Table 6 FEA results

Result	Value	Unit
Normal stress	6.132	MPa
Shear stress	2.365	MPa
Deformation	2.9	mm
Maximum principal stress	6.396	MPa
Minimum principal stress	-11.74	MPa
Maximum shear stress	0.673	MPa

Figure 11 demonstrates the comparison of the resulting FEA with the empirical computation comparison. However, the error value between the two methods that have been implemented indicates that it requires further optimization of the theoretical computational model and equalizing complex assumptions to achieve robust computational results.

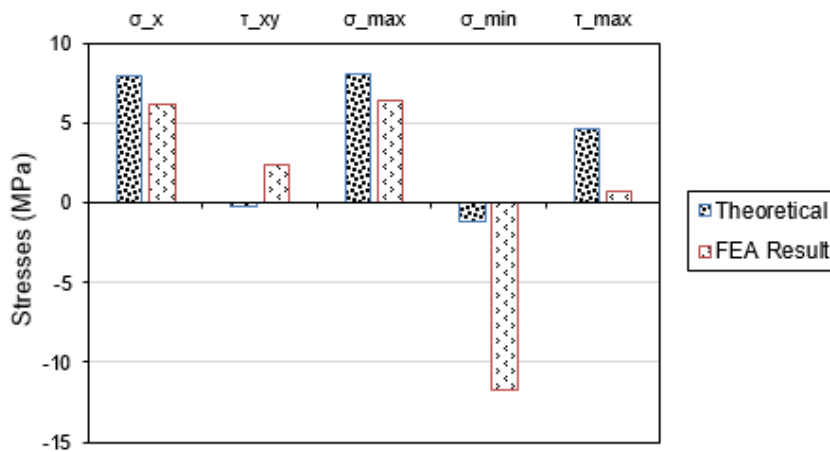


Figure 11 FEA and theoretical (empirical) stresses comparison on shell taper-less blade laminate

If the simulated normal and shear stresses (regardless of the transverse stress) are plotted in the failure envelope that has been formed (Figure 12), it is evident that the stress scatter point is in the failure envelope. This suggests that the composite design of the taper-less wind turbine blade structure is safe and can be applied.

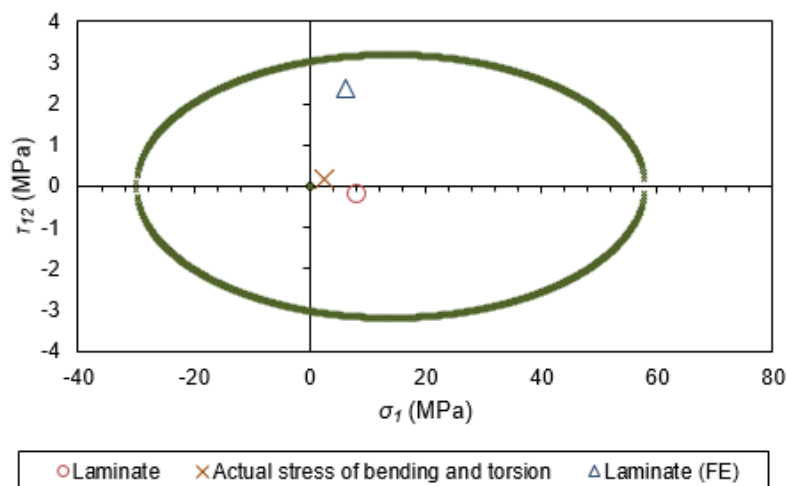


Figure 12 Hoffman's failure envelopes on the results of numerical finite element simulations and theoretical computation

The significant difference only occurs under shear stress. In theoretical computations, shear stresses are assumed to occur and are calculated on a two-dimensional plane using the average stress method of each lamina. Meanwhile, in the FEA numerical simulation, discretization uses a three-dimensional approach that accumulates shear stresses between the laminae, which results in significantly different shear stresses. It also will not have a substantial impact on the blade design that has been designed because the stress values obtained from this FEA are still in the failure envelope locus, which indicates that the design is safe. However, the transverse stress in the FEA might not be the same as the assumed constant in theoretical computations.

4. Conclusions

The optimization of lamina orientation on taper-less shell blade laminate has been done. The optimized laminate stacking sequence $[-4^\circ, 24^\circ, 47^\circ, 65^\circ, 74^\circ, 79^\circ]_S$ delivers safety factors of 7.296 and 18.057 on the longitudinal axis and the laminate plane, respectively, when experiencing a bending moment of 17.15 Nm and torque of 25.5 Nm. With a constant allowable transverse stress of -1.57 MPa, maximum allowable stress of 57.8 MPa on the longitudinal axis, and a 3.187 MPa of shear in-plane, the composite laminate is safe, both theoretically and numerically (finite element). Hence, future projects can apply the novel ramie-reinforced PLA-optimized laminate for taper-less wind turbine blades preparations. However, there is still an errors value between the two methods that have been employed. This indicates that it requires further optimization of the theoretical computational model and equalizes complex assumptions to achieve robust computational results.

Acknowledgements

Ministry of Research, Technology, and Higher Education of Republic Indonesia has funded this research under PMDSU (Pendidikan Magister menuju Doktor untuk Sarjana Unggul) Program through NKB-373/UN2.RST/HKP.05.00/2021 contract number.

References

- Al-Fatlawi, A., Jármai, K., Kovács, G., 2021. Optimal Design of a Fiber-Reinforced Plastic Composite Sandwich Structure for the Base Plate of Aircraft Pallets in Order to Reduce Weight. *Polymers*, Volume 13(5), pp. 2–36
- Baghaei, B., Skrifvars, M., Berglin, L., 2015. Characterization of Thermoplastic Natural Fibre Composites Made from Woven Hybrid Yarn Prepregs with Different Weave Pattern. *Composites Part A: Applied Science and Manufacturing*, Volume 76, pp. 154–161
- Bathias, C., Lai, D., Soemardi, T., 1992. Static and Fatigue Biaxial Testing of Fiber Composites using Thin Walled Tubular Specimens. In: *Inelastic Deformation of Composite Materials*, George J. Dvorak (ed), Springer-Verlag, New York, pp. 161–169
- Bharathiraja, G., Jayabal, S., Kalyana Sundaram, S., 2017. Gradient-Based Intuitive Search Intelligence for the Optimization of Mechanical Behaviors in Hybrid Bioparticle-Impregnated Coir-Polyester Composites. *Journal of Vinyl and Additive Technology*, Volume 23(4), pp. 275–283
- Fatra, W., Rouhillahi, H., Helwani, Z., Zulfansyah, Asmura, J., 2016. Effect of Alkaline Treatment on the Properties of Oil Palm Empty Fruit Bunch Fiber-Reinforced Polypropylene Composite. *International Journal of Technology*, Volume 7(6), pp. 1026–1034.

- Feng, N.L., Malingam, S.D., Jenal, R., Mustafa, Z., Subramonian, S., 2020. A Review of the Tensile and Fatigue Responses of Cellulosic Fibre-Reinforced Polymer Composites. *Mechanics of Advanced Materials and Structures*, Volume 27(8), pp. 645–660
- Ghasemi, A.R., Mohandes, M., 2016. Composite Blades of Wind Turbine: Design, Stress Analysis, Aeroelasticity, and Fatigue. *Wind Turbines-design, Control and Applications*, pp. 1–26
- Glinka, G., Wang, G., Plumtree, A., 1995. Mean Stress Effects in Multiaxial Fatigue. *Fatigue & Fracture of Engineering Materials & Structures*, Volume 18, pp. 755–764
- Hesty, N.W., Cendrawati, D.G., Nepal, R., Al Irsyad, M.I.A., 2021. Energy Potential Assessments and Investment Opportunities for Wind Energy in Indonesia. Centre for Applied Macroeconomic Analysis (CAMA) Working Paper, March 2021
- Kalagi, G.R., Patil, R., Nayak, N., 2018. Experimental Study on Mechanical Properties of Natural Fiber Reinforced Polymer Composite Materials for Wind Turbine Blades. *Materials Today: Proceedings*, Volume 5(1), pp. 2588–2596
- Kaw, A.K., 2006. *Mechanics of Composite Materials (Second ed.)*. Boca Raton, FL: CRC press
- Lee, C.S., Hwang, W., Park, H.C., Han, K.S., 1999. Failure of Carbon/Epoxy Composite Tubes Under Combined Axial and Torsional Loading 1. Experimental Results and Prediction of Biaxial Strength by the Use of Neural Networks. *Composites Science and Technology*, Volume 59(12), pp. 1779–1788
- Li, M., Pu, Y., Thomas, V.M., Yoo, C.G., Ozcan, S., Deng, Y., Nelson, K., Ragauskas, A.J., 2020. Recent Advancements of Plant-Based Natural Fiber-Reinforced Composites and Their Applications. *Composites Part B: Engineering*, Volume 200, <https://doi.org/10.1016/j.compositesb.2020.108254>
- Lololau, A., 2021. Mechanics Analyses and Failure of Ramie/Polylactic Acid Natural Composite Under Multiaxial Loading. Master's Thesis, Graduate Program, Universitas Indonesia, Depok
- Mahboob, Z., Bougherara, H., 2018. Fatigue of Flax-Epoxy and Other Plant Fibre Composites: Critical Review and Analysis. *Composites Part A: Applied Science and Manufacturing*, Volume 109, pp. 440–462
- Mishnaevsky, L., Branner, K., Petersen, H.N., Beauson, J., McGugan, M., Sørensen, B.F., 2017. Materials for Wind Turbine Blades: An Overview. *Materials*, Volume 10(11), pp. 1–24
- Narsai, M., Adali, S., Veale, K., Padayachee, J., 2018. Composite Tube Testing and Failure Theory Computational Comparison. *R&D Journal*, Volume 34, pp. 37–43
- National Weather Service Portland, nd. Estimating Wind Speeds with Visual Clues. *Estimating Wind*. Available Online at <https://www.weather.gov/pqr/wind>
- Ockfen, A.E., Matveev, K.I., 2009. Aerodynamic Characteristics of NACA 4412 Airfoil Section with Flap in Extreme Ground Effect. *International Journal of Naval Architecture and Ocean Engineering*, Volume 1(1), pp. 1–12
- Pickering, K.L., Efendy, M.G.A., Le, T.M., 2016. A Review of Recent Developments in Natural Fibre Composites and Their Mechanical Performance. *Composites Part A: Applied Science and Manufacturing*, Volume 83, pp. 98–112
- Piggott, H., 1997. *Windpower Workshop. Building Your Own Wind Turbine*. Centre for Alternative Technology, UK
- Quaresimin, M., Carraro, P., Maragoni, L., 2015. Influence of Load Ratio on the Biaxial Fatigue Behaviour and Damage Evolution in Glass/Epoxy Tubes under Tension-Torsion Loading. *Composites Part A: Applied Science and Manufacturing*, Volume 78, pp. 294–302
- Rajeshkumar, G., Seshadri, S.A., Devnani, G., Sanjay, M., Siengchin, S., Maran, J.P., Al-Dhabi, N.A., Karuppiah, P., Mariadhas, V.A., Sivarajasekar, N., 2021. Environment Friendly,

- Renewable and Sustainable Poly Lactic Acid (PLA) Based Natural Fiber Reinforced Composites–A Comprehensive Review. *Journal of Cleaner Production*, Volume 310, <https://doi.org/10.1016/j.jclepro.2021.127483>
- Ravianto, R., 2021. Manufacturing of Taperless-type Horizontal Axis Wind Turbine (HAWT) Blade Using Naca 6412 Airfoil With 500 W Power. Field Practical Work Report. Mechanical Engineering, Politeknik Negeri Jember.
- Rohan, T., Tushar, B., Mahesha, G.T., 2018. Review of Natural Fiber Composites. *In: IOP Conference Series: Materials Science and Engineering*, pp. 1–8
- Saidah, A., 2004. Study on product development of LPG gas cylinders with a 6 kg capacity made from ramie fiber-epoxy composites. Master's Thesis, Graduate Program, Universitas Indonesia, Depok.
- Satwika, N.A., Hantoro, R., Septyaningrum, E., Mahmashani, A., 2019. Analysis of Wind Energy Potential and Wind Energy Development to Evaluate Performance of Wind Turbine Installation in Bali, Indonesia. *Journal of Mechanical Engineering and Sciences*, Volume 13(1), pp. 4461–4476
- Sawpan, M.A., Pickering, K.L., Fernyhough, A., 2007. Hemp Fibre Reinforced Poly(lactic acid) Composites. *Advanced Materials Research*, Volume 36, pp. 337–340
- Shieddieque, A.D., Mardiyati, R.S., Widyanto, B., 2021. Preparation and Characterization of Sansevieria trifasciata Fiber/High-Impact Polypropylene and Sansevieria trifasciata Fiber/Vinyl Ester Biocomposites for Automotive Applications. *International Journal of Technology*, Volume 12(3), pp. 549–560
- Surip, S.N., Raihan, W., Jaafar, W., 2018. Comparison Study of the Bio-degradation Property of Polylactic Acid (PLA) Green Composites Reinforced by Kenaffibers. *International Journal of Technology*, Volume 9(6), pp. 1205–1215
- Suryaneta., 2007. Performance Ramie Fiber as Reinforcement in Polymer Composite for Bulletproof Panel. Bachelor's Thesis, Graduate Program, Universitas Indonesia, Depok
- Varsavas, S.D., Kaynak, C., 2018. Weathering Degradation Performance of PLA and its Glass Fiber Reinforced Composite. *Materials Today Communications*, Volume 15, pp. 344–353
- Yohana, E., Sinaga, N., Haryanto, I., Taufik, V., Dharmawan, E., 2020. Taperless Type Blade Design with Naca 5513 Airfoil for Wind Turbine 500 TSD. *In: IOP Conference Series: Earth and Environmental Science*, pp. 1–9
- Yu, T., Hu, C., Chen, X., Li, Y., 2015. Effect of Diisocyanates as Compatibilizer on the Properties of Ramie/Poly(Lactic Acid) (PLA) Composites. *Composites Part A: Applied Science and Manufacturing*, Volume 76, pp. 20–27
- Zhou, N., Yao, L., Liang, Y., Yu, B., Ye, M., Shan, Z., Qiu, Y., 2013. Improvement of Mechanical Properties of Ramie/Poly (Lactic Acid) (PLA) Laminated Composites using a Cyclic Load Pre-Treatment Method. *Industrial Crops and Products*, Volume 45, pp. 94–99